Acid-Induced Dissolution of Andesite: Evolution of Permeability and Strength

Jamie Farquharson, Bastien Wild, Alexandra Kushnir, Michael Heap, Patrick Baud, Ben Kennedy

JGR Solid Earth

RESEARCH ARTICLE
10.1029/2018JB016130

Acid-Induced Dissolution of Andesite: Evolution of Permeability and Strength

Jamie I. Farquharson[1,2], Bastien Wild[3,4], Alexandra R. L. Kushnir[1], Michael J. Heap[1], Patrick Baud[1], and Ben Kennedy[5]

[1]Géophysique Expérimentale, Institut de Physique de Globe de Strasbourg (UMR 7516 CNRS, Université de Strasbourg/EOST), Strasbourg, France, [2]Rosenstiel School of Marine and Atmospheric Sciences, University of Miami, Miami, FL, USA, [3]Laboratoire d'Hydrologie et de Géochimie de Strasbourg (UMR 7517 CNRS, Université de Strasbourg/EOST), Strasbourg, France, [4]Andlinger Center for Energy and the Environment, Princeton University, Princeton, NJ, USA, [5]Geological Sciences, University of Canterbury, Christchurch, New Zealand

Key Points:
- Volcanic environments often host strongly acidic lakes or aquifers
- Prolonged exposure of andesite to sulfuric acid induces mineral dissolution
- As a consequence, permeability and porosity increase, while mass decreases

Correspondence to:
J. I. Farquharson,
jifarq89@googlemail.com

Citation:
Farquharson, J. I., Wild, B., Kushnir, A. R. L., Heap, M. J., Baud, P., & Kennedy, B. (2019). Acid-induced dissolution of andesite: Evolution of permeability and strength. *Journal of Geophysical Research: Solid Earth*, *124*, 257–273. https://doi.org/10.1029/2018JB016130

Received 21 MAY 2018
Accepted 23 DEC 2018
Accepted article online 1 JAN 2019
Published online 17 JAN 2019

Abstract Volcanic systems often host crater lakes, flank aquifers, or fumarole fields that are strongly acidic. In order to explore the evolution of the physical and mechanical properties of an andesite under these reactive chemical conditions, we performed batch reaction experiments over timescales from 1 day to 4 months. The experiments involved immersion of a suite of samples in a solution of 0.125 M sulfuric acid (pH ~0.6). Periodically, samples were removed and their physical and mechanical properties measured. We observe a progressive decrease in mass, coincident with a general increase in porosity, which we attribute to plagioclase dissolution accompanied by the generation of a microporous diktytaxitic groundmass due to glass dissolution. Plagioclase phenocrysts are seen to undergo progressive pseudomorphic replacement by an amorphous phase enriched in silica and depleted in other cations (Na, Ca, and Al). In the first phase of dissolution (t = 24–240 hr), this process appears to be confined to preexisting fractures within the plagioclase phenocrysts. However, ultimately these phenocrysts tend toward entire replacement by amorphous silica. We propose that the dissolution process results in the widening of pore throats and the improvement of pore connectivity, with the effect of increasing permeability by over an order of magnitude relative to the initial measurements. Compressive strength of our samples was also modified, insofar as porosity tends to increase (associated with a weakening effect). We outline broader implications of the observed permeability increase and strength reduction for volcanic systems including induced flank failure and related hazards, improved efficiency of volatile migration, and attendant eruption implications.

Plain Language Summary Where water is present in volcanic environments, it is often strongly acidic due to the presence of dissolved gases such as sulfur dioxide (involving similar process to that which forms acid rain). Indeed, it is estimated that almost 800 acidic volcanic lakes exist worldwide. In terms of volcanic hazard it is important to understand the influence of such acids on volcanic rocks. We performed experiments where samples of volcanic rock were submerged in an acid solution for varying lengths of time (we used a strong concentration of sulfuric acid in order to mimic the chemistry of a natural acid lake). We find that some of the minerals in our samples dissolve over time when in contact with the acid. Ultimately, this makes the rock weaker and more porous and increases the ability for fluid to flow through the rock. These results indicate that certain large-scale mechanisms might occur more frequently in nature when there are acidic conditions, such as the collapse of part of the side of the volcano or the rim of its crater. In this paper we describe the processes occurring on the microscale and outline broad implications for our results in the context of volcanic areas.

1. Introduction

Subaerial volcanic systems often host acidic crater lakes, such as those shown in Figure 1. Indeed, Perez et al. (2011) estimate the existence of some 769 volcanic lakes globally, a revised estimate based on the value of 138 reported by Delmelle and Bernard (2000). Their existence and persistence requires a regular input of water (e.g., meteoric water) at a rate that exceeds the migration of fluid from the system—for example, due to evaporation or fluid flow through the porous edifice—coupled with a relatively continuous transfer of

Figure 1. Acid lakes in volcanic environments. (a) Crater Lake, Ruapehu, New Zealand (approximately 300 × 440 m, with a pH of around 0.6; Christenson & Wood, 1993). (b) Emerald lakes, Tongariro, New Zealand (approximately 65 × 110 m, with a typical pH of around 3; Michaelis, 1982; Timperley & Vigor-Brown, 1986). (c) Whakaari crater (White Island), New Zealand (approximately 500 × 275 m, with a pH ranging from around 1.5 to less than −1; Christenson et al., 2017). (d) El Chichón, Chiapas, Mexico (approximately 370 × 470 m, with a typical pH range of 0.5–3.0; Armienta et al., 2000; Casadevall et al., 1984). (Photograph used with permission from Graeme Alexander William Sinclair.) Note that the dimensions and pH of these (indeed, all) volcanic lakes fluctuate considerably over time.

magmatic volatiles and heat (e.g., Delmelle & Bernard, 1994). Crater lakes serve to trap reactive magmatic volatiles such as SO_2, H_2S, HCl, and HF, commonly resulting in a highly acidic composition: pH values of around 0.6 or lower are common in volcanic lakes around the globe (e.g., Armienta et al., 2000; Bernard et al., 2004; Casadevall et al., 1984; Christenson & Wood, 1993; Delmelle & Bernard, 1994; Lowenstern et al., 2018; Rouwet et al., 2008; Varekamp et al., 2000). One of the most prevalent acid agents is sulfuric acid (H_2SO_4), which may be derived either from the disproportionation of volatile SO_2 via hydrolysis (e.g., de Moor et al., 2016; Kusakabe et al., 2000):

$$3\ \ SO_2 + 2\ \ H_2O \leftrightharpoons S + 2H_2SO_4^- + 2\ \ H^+ \tag{1}$$

or

$$4\ \ SO_2 + 4\ \ H_2O \leftrightharpoons 3\ \ H_2SO_4 + H_2S, \tag{2}$$

or from the hydrolysis of elemental sulfur:

$$4\ \ S + 4H_2O \rightarrow 3H_2S + H_2SO_4 \tag{3}$$

all of which are common processes in volcanic environments.

Given that volcanic rocks are often immersed in or exposed to H_2SO_4, it is important to understand the influence a reactive chemical environment may have on the physical and mechanical properties of edifice-forming materials. Indeed, Hemley and Jones (1964) highlight that the presence of sulfur compounds in hypogene solutions is one of the most crucial parameters governing alteration of silicate materials. In magma and in the rocks that form a volcanic edifice, porosity (the fraction of void space within a material)

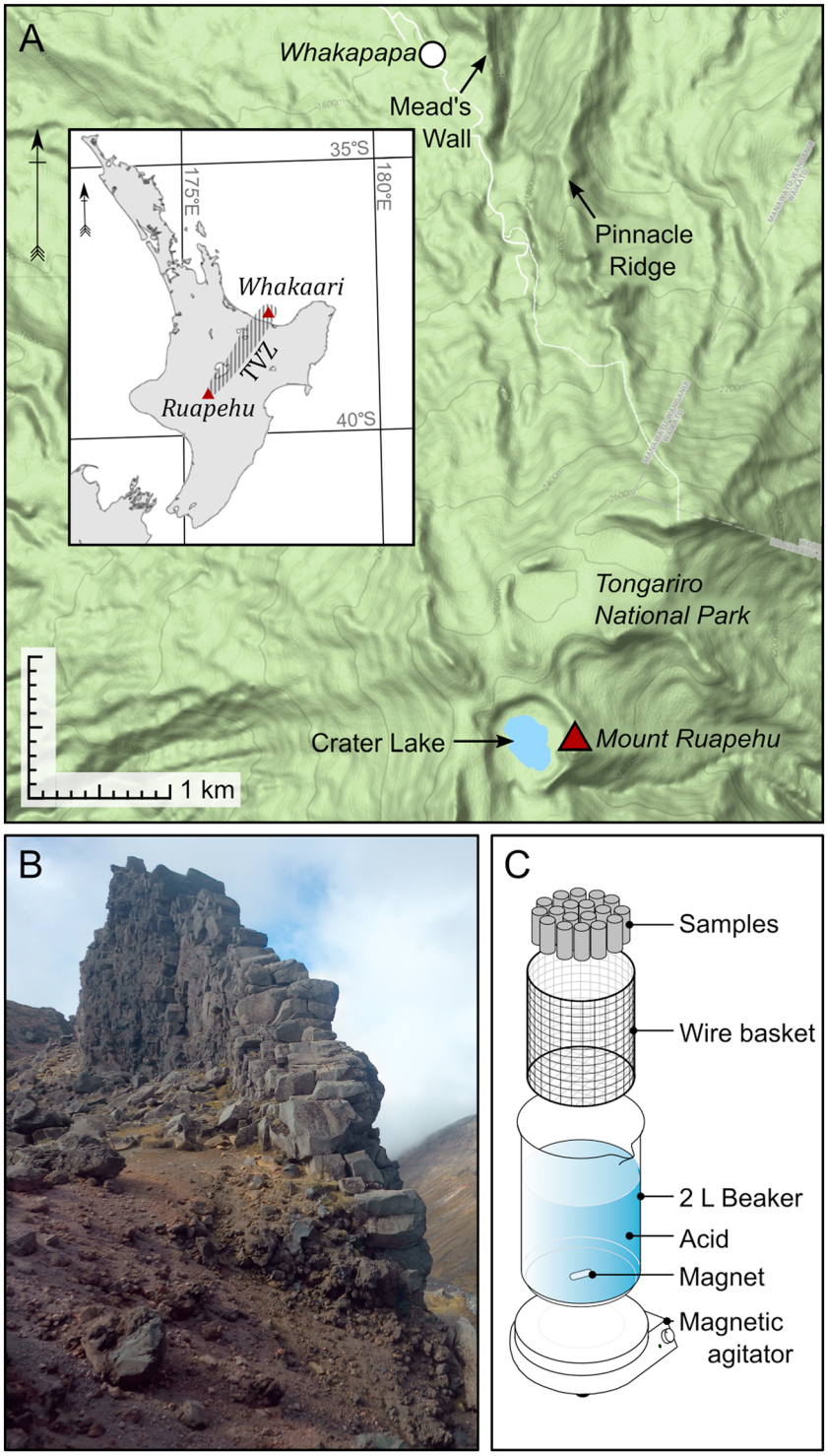

Figure 2. Sampling location and experimental setup. (a) Location of Mead's Wall dyke with respect to Mount Ruapehu and the Taupō Volcanic Zone (TVZ: *inset*). Map data © 2018 Google. (b) Photograph of Mead's Wall dyke, near the village of Whakapapa, New Zealand. Dyke width varies between 2.5 and 3.5 m; exposed length is approximately 100 m. (c) Diagram of experimental acid immersion setup.

and permeability (the capacity for fluid to flow through that porosity) are critical properties determining volatile migration and pressure evolution in active volcanic systems. It is generally understood that efficient mechanisms of outgassing—facilitated by high permeability—may preclude the generation of overpressure in magma and in turn reduce the potential for explosive eruptions at any given volcano. Conversely, if the permeability of the volcanic system is generally low, this may foster pressure buildup, which can in turn drive explosive activity (Sparks, 1978): a concept that underlies numerous theoretical, experimental, and numerical studies in volcanology (e.g., Ashwell et al., 2015; Edmonds & Herd, 2007; Eichelberger et al., 1986; Nguyen et al., 2014; Okumura & Sasaki, 2014; Rust et al., 2004; Woods & Koyaguchi, 1994). Moreover, the evolution of these properties over time can result in an attendant change in pressure and thus explosive potential (Farquharson, Wadsworth, et al., 2017). Similarly, the failure strength of edifice-forming rock (and other related mechanical properties) can dictate the potential for volcanic flank collapse and associated volcanic hazards. The capacity for edifice weakening or strengthening over time is thus an important consideration (e.g., Reid et al., 2010), and previous research has highlighted the important contribution of alteration to the strength and stability of volcanic edifice and dome structures (e.g., Ball et al., 2013, 2015; Reid et al., 2001). In volcanic systems around the world, alteration-induced edifice weakening has been related to consequent generation of potentially devastating collapse and flow phenomena (e.g., Carrasco-Núñez et al., 1993; Cook et al., 2017; Houghton et al., 1987; Manville et al., 2007; Neall, 1976; Varekamp et al., 2001). In this contribution, we examine the evolution of physical and mechanical properties of a volcanic rock when immersed in acid, analogous to the reactive aqueous chemical environment encountered in acid lake-hosting volcanic systems.

2. Materials and Methods

The starting material for this experimental study was collected from a massive dyke outcrop on the northern flank of Mount Ruapehu, New Zealand. The site is culturally and ecologically protected and sampling was confined to a single small hand sample (approximately $10 \times 10 \times 30$ cm) leaving no trace of sampling in line with sample permit guidelines and cultural consideration. Mead's Wall dyke (Figures 2a and 2b) exhibits the NNE-SSW strike line common to other exposed volcanic structures in the region (such as Pinnacle Ridge: Figure 2a) and echoes the orientation of active and historically active volcanic vents in the Tongariro Volcanic Centre and the Taupō Volcanic Zone in general. This trend is attributed to the alignment of the regional stress field (e.g., Nakamura, 1977). The dyke has been uncovered by regional glaciation, and over time, fragments have spalled from the exposed surfaces; the hand sample used in this study was one of these spalled samples. X-ray powder diffraction (XRPD) was performed on a powdered sample in order to identify mineral phases of the Mead's Wall andesite, comprised primarily of plagioclase feldspar ($67\% \pm 3\%$), pyroxene ($28\% \pm 4\%$), cristobalite ($3\% \pm 2\%$), and titanomagnetite ($2\% \pm 1\%$). These phases were confirmed using energy-dispersive X-ray analysis (EDX) and are in general agreement with the results of O'Shea (1957), who examined the same dyke outcrop. Figure 3 shows typical microstructure of an as-collected sample. The material is a porphyritic andesite, characterized by abundant plagioclase feldspar—ranging from Na-rich andesine to Ca-rich bytownite—and clinopyroxene phenocrysts within a crystalline groundmass. As highlighted in Figures 3a and 3b, the phenocrysts tend to be euhedral, pervasively fractured, and often host inclusions. Cristobalite occurs primarily within pores (e.g., Figures 3a and 3c) and is easily recognized by its characteristic "fish scale" cracking, indicative of the material having undergone the β- to α-cristobalite transition (e.g., Damby et al., 2014; Horwell et al., 2013; Kushnir et al., 2016).

Samples (40 mm in length and 20 mm in diameter) were cored, precision-ground, and dried for a minimum of 48 hr at 40 °C until they attained a constant mass (i.e., to ensure the removal of any residual moisture within the pores). Helium pycnometry and gas permeametry were used to determine their connected porosity φ and permeability k, respectively. A combination of the permeant used (nitrogen gas) and characteristics of the pore structure meant that an ancillary correction was required for the measured permeability data (see Klinkenberg, 1941; McPhee & Arthur, 1991), such that

$$k = k_{\infty}\left(1 + \frac{b}{\bar{p}}\right) \tag{4}$$

where k_{∞} is the "inert liquid permeability", that is, the value of permeability that would be obtained in the absence of gas slippage by using an inert liquid permeant (e.g., McPhee & Arthur, 1991). The value $\bar{p}$ is the mean gas pressure across the sample during measurement, and b is the so-called Klinkenberg slip

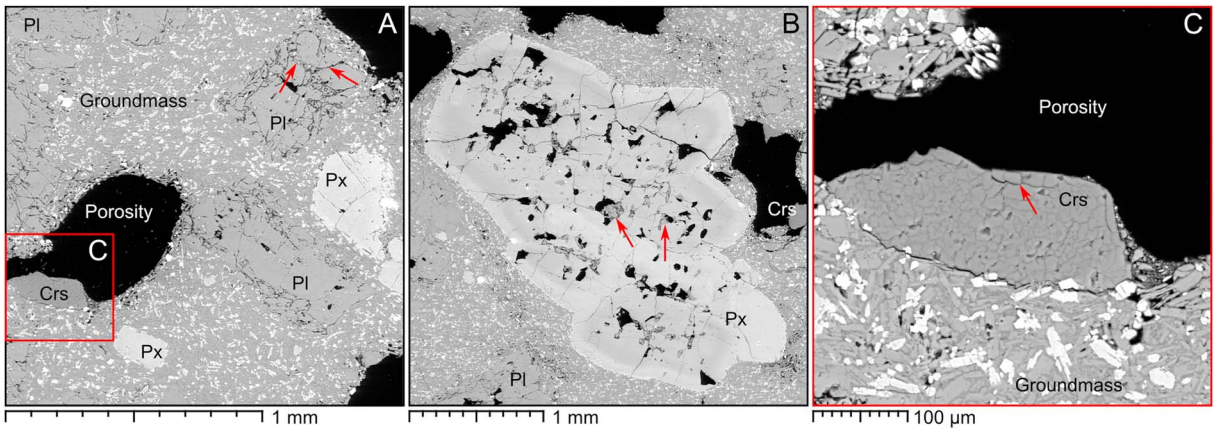

Figure 3. Microstructural characteristics of Mead's Wall andesite, the starting material for our experiments. (a) Abundant large phenocrysts of plagioclase (Pl) and pyroxene (Px) are hosted within a crystalline groundmass. Porosity, shown in black, exists in the form of large (>500-μm diameter) pores, intercrystalline microporosity (<30μm), and ubiquitous microfractures. The plagioclase crystals are often pervasively fractured, as highlighted by the arrows. (b) Pyroxene are also often fractured and sometimes contain inclusions of plagioclase, highlighted by the arrows in this panel. (c) Detail of cristobalite (Crs), which is found throughout these samples, almost exclusively within pores. Arrow highlights the so-called "fish-scale" cracking. Bright white spots are crystals of Mg- and Al-bearing titanomagnetite.

factor (McPhee & Arthur, 1991). All measurements were performed under 1 MPa confining pressure at room temperature. Additional measurement and correction procedures are described in detail by Heap, Kushnir, et al. (2017). Hereafter, all reported permeability values are the "true", Klinkenberg-corrected, data. We arbitrarily define a threshold for determining whether to apply the above correction to our data, when the slope of permeability k versus the reciprocal of the mean pressure $\bar{p}^{-1}$ exhibited an r^2 value of 0.99 or greater, based on standard least squares regression (see Farquharson, Baud, & Heap, 2017). In practice, all of the andesites of this study fulfilled this criterion.

Nine of the 19 samples were set aside in order to measure their uniaxial compressive strength (UCS), which was measured under saturated conditions in a water bath at a strain rate of 10^{-5} s^{-1}. A schematic of the deformation apparatus used is described in Heap et al. (2014). The remaining samples were immersed in a batch reactor filled with 0.125 M solution of H_2SO_4 at 22.9 ± 0.7 °C (with a starting pH of 0.64: a reasonable value for volcanic acid lakes), with samples being removed at intervals in order to recharacterize their physical and mechanical properties (mass m, porosity φ, permeability k, and compressive strength). The acid was constantly stirred using a magnet and magnetic agitator, as depicted in Figure 2c. The wire basket was composed of Grade 304 stainless steel, with a sulfuric acid corrosion rate—under the imposed temperature and concentration conditions—of well below the 0.1-mm/year threshold for acceptable material performance. Similarly, the magnet and beaker were assumed not to affect the dissolution process over the time frame of our experiments. Nogami and Yoshida (1995) were able to unravel the temperature dependence of the overall dissolution process of basaltic andesite (from Mihara-Yama volcano on the Japanese island of Izu Ōshima) in an acid environment. Moreover, these authors demonstrate that the reaction mechanisms are identical at temperatures up to at least 160 °C, so we may be confident that results of the room temperature experiments shown herein are representative of the mechanisms operative in natural systems, where there is the potential for much higher temperatures. In our study, cylindrical samples were used rather than relatively more reactive powder or chips, in order that their bulk physical and mechanical properties could be investigated before and after acid immersion. Five additional blocks of Mead's Wall andesite, each approximately 30 × 60 × 10 mm, were also included in the acid batch. These were removed after 24, 72, 240, 600, and 1,944 hr, respectively (i.e., 1, 3, 10, 25, and 81 days); thin sections were prepared from these in order that any evolution of the sample microstructure or chemistry could be observed using scanning electron microscopy (SEM) and EDX. Samples were embedded in epoxy resin, trimmed, and

Table 1
Connected Porosity φ and Uniaxial Compressive Strength (UCS) of Select Andesite Samples (Samples Not Subject to Acid Immersion)

Sample	φ	UCS (MPa)
MW-1	0.171	56.54
MW-3	0.190	53.36
MW-7	0.206	49.70
MW-9	0.144	74.27
MW-12	0.131	78.07
MW-13	0.198	50.69
MW-15	0.160	71.68
MW-16	0.193	57.14
MW-20	0.189	53.77

Table 2
Physical and Mechanical Properties of Andesites that Underwent Acid Immersion

Sample	t (hr)	φ	φ^*	$\Delta\varphi$	k (m^2)	k^* (m^2)	m (g)	m^* (g)	Δm	UCS (MPa)
MW-2	24	0.193	0.195	0.003	9.30×10^{-18}	9.74×10^{-18}	28.942	28.852	−0.090	55.45
MW-4	48	0.182	0.187	0.006	2.79×10^{-17}	3.51×10^{-17}	29.370	29.228	−0.142	58.81
MW-5	72	0.176	0.178	0.003	8.94×10^{-18}	2.56×10^{-17}	29.777	29.624	−0.153	54.66
MW-6	120	0.184	0.191	0.007	5.61×10^{-17}	9.89×10^{-17}	29.364	29.141	−0.223	55.31
MW-8	240	0.168	0.178	0.011	7.89×10^{-18}	2.40×10^{-17}	29.856	29.505	−0.351	60.81
MW-11	384	0.192	0.198	0.006	2.32×10^{-17}	6.47×10^{-17}	29.182	28.778	−0.404	57.38
MW-14	600	0.186	0.196	0.010	9.14×10^{-18}	2.33×10^{-17}	29.362	28.758	−0.604	50.78
MW-17	1,008	0.184	0.190	0.006	2.11×10^{-17}	7.37×10^{-17}	29.447	28.735	−0.712	50.77
MW-18	1,944	0.164	0.163	−0.001	2.71×10^{-17}	6.49×10^{-17}	30.253	29.484	−0.769	58.15
MW-19	2,880	0.193	0.201	0.007	7.70×10^{-18}	1.64×10^{-16}	29.066	28.168	−0.898	50.86

Note. φ = initial porosity; φ^* = final porosity; $\Delta\varphi$ = porosity change; k = initial permeability; k^* = final permeability; m = initial mass; m^* = final mass; Δm = mass change; UCS = postimmersion uniaxial compressive strength; t = total acid immersion time.

polished to produce thin sections, which were then carbon coated. EDX spectra were collected at several point locations across each thin section at 30-kV accelerating voltage, with the probe current and spot size adjusted so as to obtain dead times in the optimal range of 30–40%.

3. Results

3.1. Physical and Mechanical Property Evolution

Throughout the rest of this study, we will present physical property data such that a for a given property corresponds to the preimmersion value, a^* is the postimmersion value, and a' is the relative change in the value of that property such that $a' = a/a^*$. Further, $\Delta a = a^* - a$. Table 1 shows the connected porosity φ and UCS of the sample suite that did not undergo acid stimulation. Table 2 shows the preimmersion and postimmersion values of connected porosity, sample mass, and gas permeability of the acid-stimulated samples, as well as their postimmersion compressive strength. The final column t shows the total acid immersion time of each sample.

The experimental data are shown graphically in Figure 4. All normalized data (Figures 4a–4c) are shown relative to 1 at time 0. Values > 1 indicate an increase in that property relative to the initial value, and values <1 indicate a decrease relative to the initial value. Figure 4a illustrates the normalized mass change m' over time, which decreases to less than 0.97 after 2,880 hr (representing a 3% total mass loss from the sample). Figure 4b shows normalized sample porosity φ' versus immersion time. Values range from 1.06 to just less than 1, representing an increase by up to 6% in porosity in some samples, and a decrease (by <1%) in another. Error bars represent the propagated uncertainty due to imperfect sample geometry (see Farquharson, Baud, & Heap, 2017, for details). Figure 4c shows permeability increase over time, with k' reaching as high as 21.27 after the maximum immersion time (2,880 hr). Finally, Figure 4d shows UCS as a function of connected porosity for both the acid-treated and untreated sample suites (in the case of the latter, the porosity is the postimmersion porosity φ^*). The samples that have undergone acid immersion do not deviate significantly nor systematically from this trend. Notably, the UCS-φ trend exhibited by these data are in line with previous measurements on andesite sampled from the same dyke by Massiot (2017; see Figure 4d).

3.2. Postimmersion Microstructure

Figures 5b–5f show SEM images of Mead's Wall andesites immersed in H_2SO_4 for progressively longer time periods, with Figure 5a being an untreated sample for reference. For $t = 0$ and $t = 24$ hr (Figures 5a and 5b), a distinct feature of the microstructure is the pervasive fracture networks visible in the plagioclase feldspar crystals (as highlighted in Figure 3). After 72 hr of immersion (Figure 5c), the development of amorphous silica (opal-A: $SiO_2 \cdot nH_2O$; see also Figure 8) is apparent. These amorphous silica surface layers (ASSLs) tend to correspond to pre-existing fractures after relatively short immersion times (72 and 240 hr: Figures 5c and 5d). However, after 600 hr and longer (Figures 5e and 5f), ASSL textures can be observed forming dissolution rinds around phenocryst boundaries and intruding toward the centers of plagioclase crystals. Note that in both Figures 5e and 5f, the original outline of the weathered plagioclase phenocryst can be easily discerned.

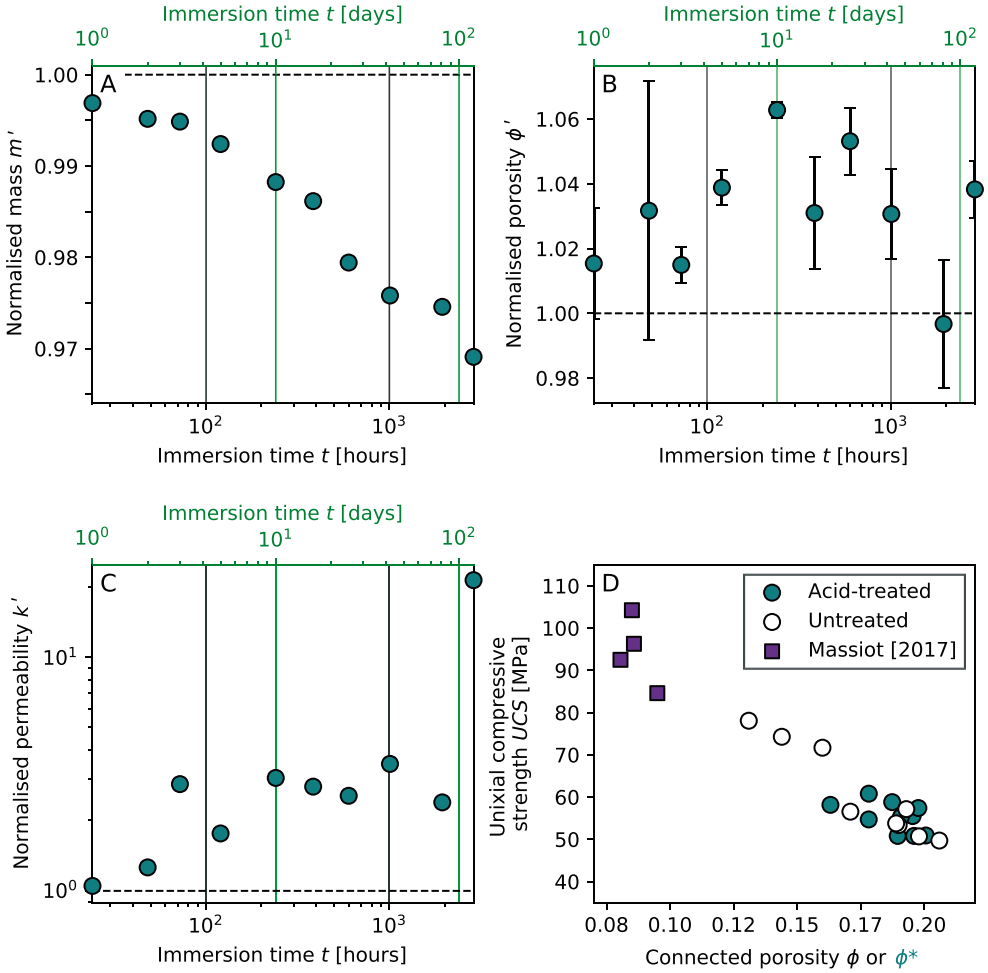

Figure 4. Experimental data. (a) Relative change in sample mass m' against immersion time. (b) Relative change in sample porosity φ' against immersion time. (c) Relative change in sample permeability k' against immersion time. (d) Connected porosity for all samples versus uniaxial compressive strength (see Tables 1 and 2). For comparison, we also show the data of Massiot (2017). In panels a–c, values >1 indicate a relative increase in mass, porosity, or permeability, whereas values <1 indicate a decrease relative to the initial values. The point at which no change is recorded is shown by the dashed line, where appropriate.

As shown in detail in Figure 6, phenocrysts of pyroxene are not visibly altered by their immersion in the experimental acid solution (over the time frame of our experiments). However, feldspar inclusions within the pyroxene phenocrysts have clearly been subject to acid-induced dissolution.

Finally, Figure 7 highlights the development of diktytaxitic microtextures within two Mead's Wall samples. All samples predominantly exhibit a porphyritic texture characterized by porosity and large phenocrysts hosted within a dense groundmass of microcrystals and andesitic glass, as was the case prior to acid immersion (Figure 3a). However, following acid treatment, the groundmass in many places appears as a randomly oriented array of tabular (lath-shaped) microlitic crystals of plagioclase and pyroxene densely packed within a glass-free mesostasis. In our samples, this texture is typically observed proximal to large pores; consequently, after dissolution, many pores are surrounded by a diktytaxitic halo with abundant interstitial microporosity. Where a pore exists more-or-less in isolation, the diktytaxitic textures radiate outward from it into the surrounding groundmass (Figure 7a). Where two or more pores are in proximity, the microporous texture tends to form bridges between them (Figure 7b). Notably, the textures described here appear to be visible throughout the sample areas studied: dissolution-induced textures do not tend to be more prevalent at the sample edges, for example.

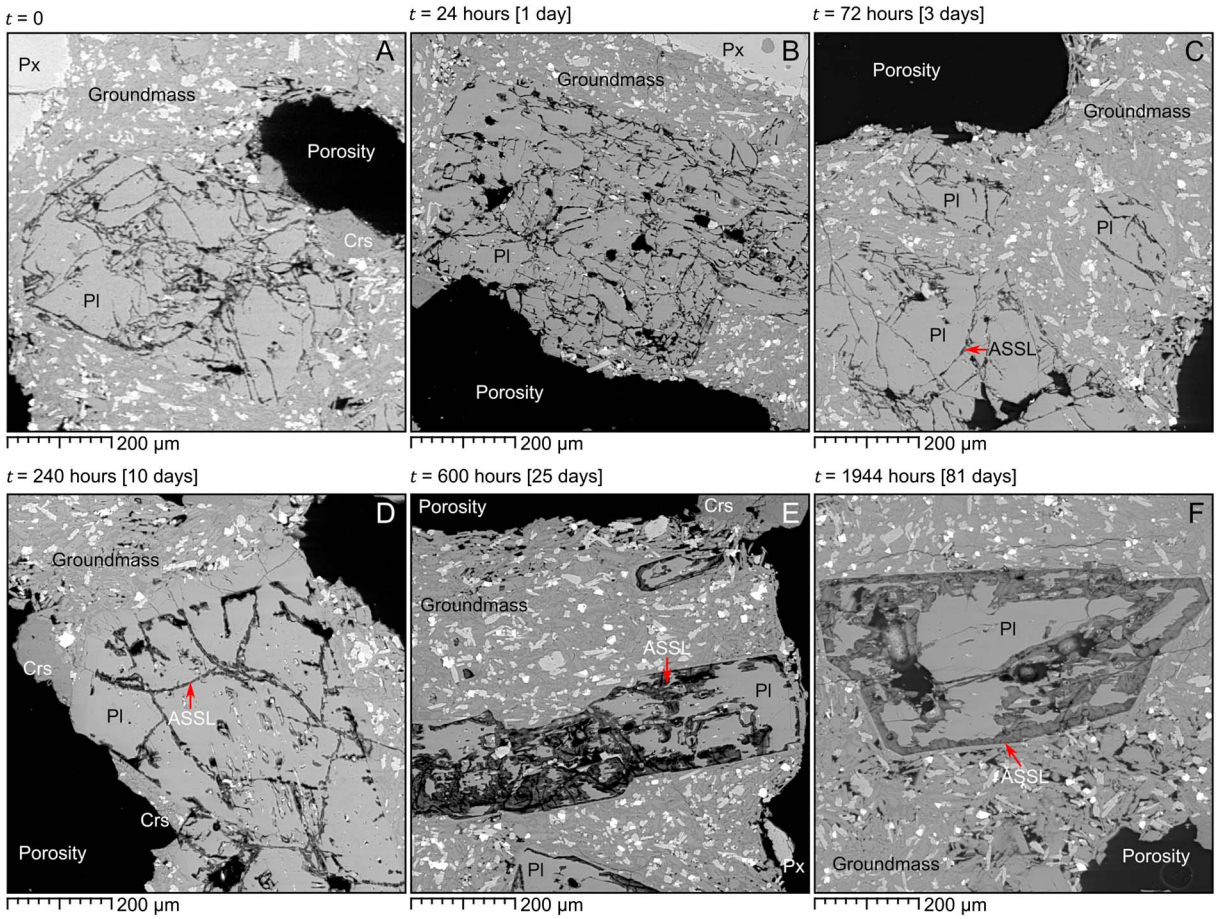

Figure 5. Progression of dissolution mechanisms over time. (a) An untreated sample of Mead's Wall andesite for reference. As in previous figures, Pl = plagioclase, Px = pyroxene, and Crs = cristobalite. Note the intense fracturing of the plagioclase phenocrysts. (b) After 24 hr, the microstructural textures remain very similar to those observed in (a). (c) After 72 hr, we observe the development of rinds of amorphous silica surface layers (ASSL) appearing in the fractured plagioclase, along the planes of preexisting fractures. (d) After 240 hr, we observe that the development of more ASSL as acid-induced dissolution further exploits preexisting fracture networks. (e) After 600 hr, dissolution has progressed to the centers of many large phenocrysts. (f) Similar dissolution textures to those seen in (d) are observed after 1,944 hr. Refer to text for discussion.

3.3. Postimmersion Chemistry

Over the first week of dissolution, pH increased from the starting value of 0.64 to a value around 0.77, whereafter it remained relatively consistent (ranging between 0.93 and 0.72 as a function of the ambient temperature) over time. Final fluid composition indicated that the solution remained undersaturated with respect to the dissolution of all primary minerals identified, signifying that conditions favorable to the dissolution of andesite were maintained throughout the experiment.

Bulk XRPD analysis of a sample having undergone acid immersion for 1,944 hr highlighted the formation of gypsum ($CaSO_4 \cdot 2H_2O$) and the presence of amorphous silica, in addition to the preexisting mineral phases. EDX analysis was used to further assess spatial distribution of amorphous silica within that same sample. Figure 8a shows a phenocryst (light gray) significantly replaced by ASSL (dark gray) after 1,944 hr of immersion in acid. White and red symbols indicate where Plagioclase and ASSL EDX spectra (Figure 8b) were respectively acquired. Figure 8b shows stacked EDX spectra normalized to Si. They highlight the dramatic change of composition that occurred during the transformation of plagioclase to amorphous silica. Ca and Al peaks are significantly reduced, while no Na could be detected in the ASSL. We note that the similarity of spectra from different plagioclase samples (not shown here) suggests that there exists negligible inherent compositional variability between phenocrysts.

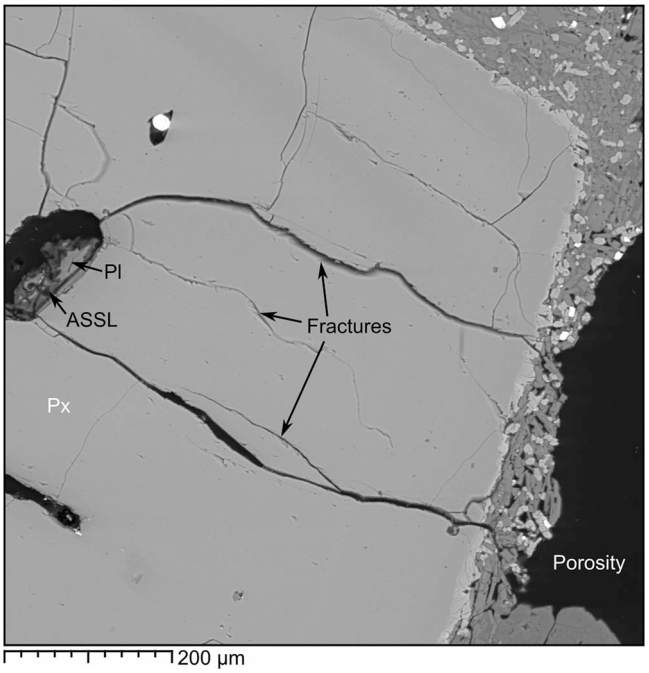

Figure 6. Detail of a large pyroxene phenocryst, in a sample immersed in H_2SO_4 for 1,944 hr (81 days). Note that the pyroxene is itself not visibly altered. However, plagioclase feldspar inclusions have been subject to acid-induced dissolution. Pl = plagioclase; Px = pyroxene; ASSL = amorphous silica surface layer. Refer to text for more details.

4. Discussion

4.1. Microstructural Evolution

The progression of phenocryst textures over time (Figure 5), along with the attendant chemistry (Figure 8), allows us to interpret the progression of dissolution mechanisms with prolonged immersion time. In the early stages (t = 24–240 hr: Figures 5b–5d), acid-induced dissolution is primarily confined to narrow pre-existing fractures within the plagioclase phenocrysts. These fractures serve as migration routes for cation release during the incongruent dissolution process leading to the precipitation of secondary amorphous silica-rich surface layers (ASSLs). The ASSLs widen over time as the reaction front propagates into the center of the crystals (e.g., Figures 5e and 5f), ultimately resulting in almost complete pseudomorphic replacement of the initial mineral by a silica-rich phase or in residual irregular patches of plagioclase within silica-rich frameworks that retain the external shapes of relict phenocrysts. Complete or partial pseudomorphic replacement of silicate minerals has been recognized in a broad range of volcanic systems, including in fumarolic deposits from Mount Usu, Japan (Africano & Bernard, 2000), ash from Sakurajima volcano, Japan (Kawano & Tomita, 2001), crater lake sediments from Mount Ruapehu, New Zealand (Christenson et al., 2010), ash from Mount Kiso Ontake, Japan (Minami et al., 2016) and Cotopaxi volcano, Ecuador (Gaunt et al., 2016), lavas from Poás, Costa Rica (Rodríguez & van Bergen, 2017), and in lavas and volcaniclastic deposits from Kawah Ijen, Indonesia (Lowenstern et al., 2018, and references therein), as well as in experimental studies (see Putnis, 2009, and references therein). In each of these cases, feldspar phenocrysts were replaced by amorphous or crystalline silica due to synemplacement or postemplacement interaction with a reactive chemical environment. Comparable textures are clearly visible in our postimmersion sample microstructure, highlighting that we were able to reproduce dissolution mechanisms observed in a number of volcanic environments.

We observe abundant cristobalite in the postimmersion microstructure (in Figures 5d and 5e, for example). However, the observation of fish scale cracking on these silica polymorphs highlights that they were preexisting in the crystal cargo in each case: cracking arises from a volumetric change associated with the transition from β- to α-cristobalite (e.g., Damby et al., 2014). Notably, this displacive transition occurs at approximately 200 °C, and our batch experiments were carried out at room temperature (22.9 ± 0.7 °C).

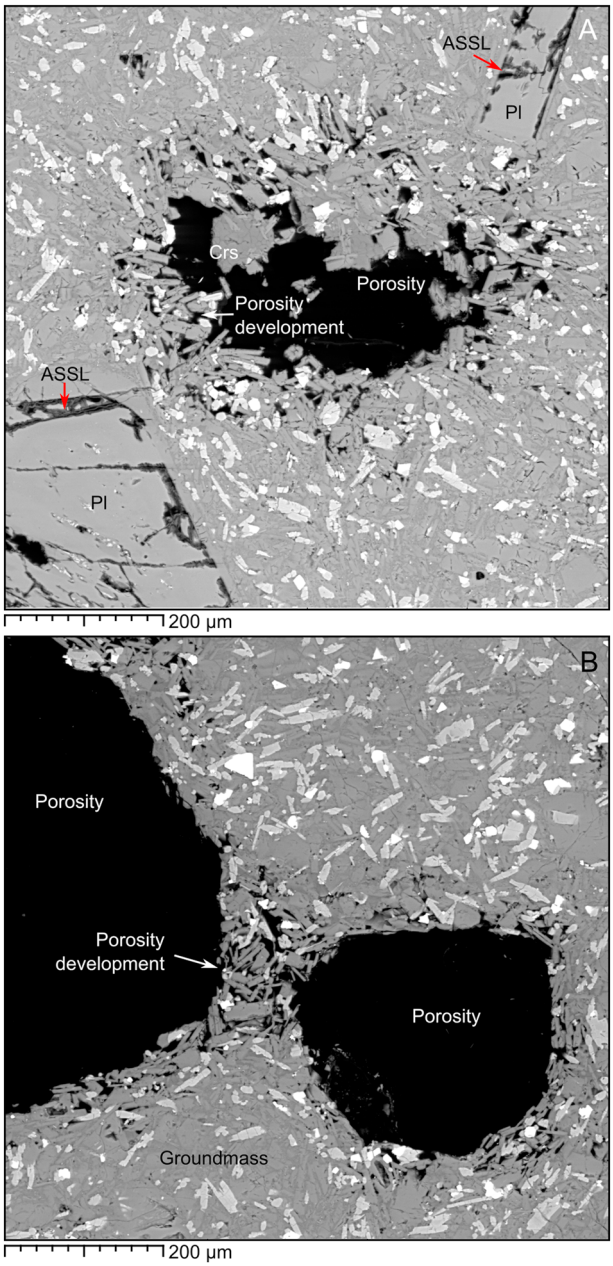

Figure 7. Microstructural evidence of pore throat widening. (a) Detail of a pore with a Mead's Wall andesite sample immersed in acid for 240 hr. Note that pore walls are not smooth; rather, dissolution of the interstitial glass proximal to the pore appears to have occurred, resulting in the development of microporosity radiating away from the pore. (b) Two large pores in a sample of Mead's Wall andesite that has undergone acid immersion for 600 hr. Note the relative abundance of intercrystalline micro-porosity surrounding both pores and in the bridging groundmass between them (highlighted by the arrow). Pl = plagioclase; ASSL = amorphous silica surface layer; Crs = cristobalite. Refer to text for more discussion.

4.2. Dissolution, Mass Loss, and Porosity Change

As shown in Figure 4a, sample mass clearly decreases with prolonged acid immersion time: the normalized mass m' drops from 1 (at time 0) to less than 0.97 after 2,880 hr (i.e., just over 3% of the initial sample mass was lost). This suggests that progressive dissolution of the andesite occurred throughout the duration of acid immersion. However, the rate at which this occurred evidently decreased over time. Notably, this continued mass loss is not reflected in a monotonic increase in connected porosity (Figure 4b). Rather, there is a significant degree of scatter in the plot of normalized porosity over time. The potential causes of this scatter are

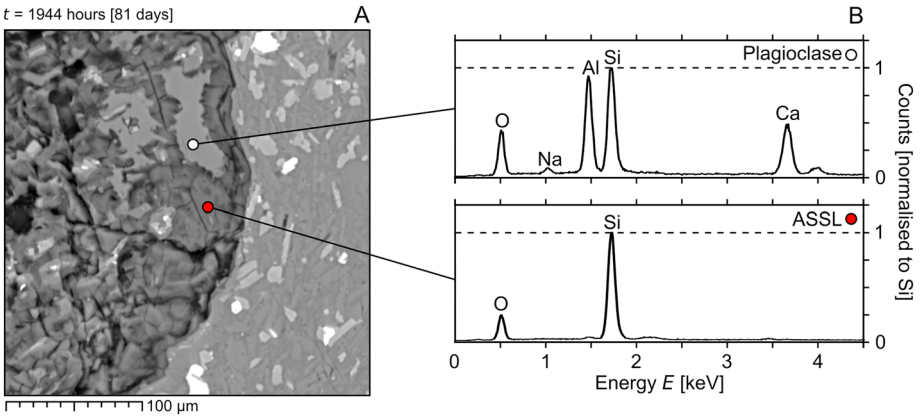

Figure 8. Energy-dispersive X-ray analysis for a select phenocryst. (a) Energy-dispersive X-ray sampling locations on a plagioclase phenocryst (white symbol) and on the amorphous silica layer (ASSL; analysis point shown by the red symbol). Panel (b) shows the derived spectra from each location. Elemental peaks are normalized to silicon (Si). O = oxygen; Na = sodium; Al = aluminum; Ca = calcium. This sample was immersed in acid for t = 1,944 hr (81 days).

both physical and experimental: first, the overall volume of connected porosity is not necessarily an accurate predictor of the connectivity and tortuosity of porous networks in volcanic rock (Colombier et al., 2017; Farquharson et al., 2015). If acid dissolution acts to widen the apertures of pore throats, for example, then this mechanism may not be proportionally reflected in the bulk porosity change measured as a function of time. Additionally, the presence of gypsum measured using XRPD is presumably due to its precipitation while samples were being dried following acid immersion: potentially influencing the measured postimmersion connected porosity. Finally, porosity is the physical property measurement (studied here) that is most prone to the introduction of experimental error. The calculation—and associated error—of connected porosity φ is described in detail in Farquharson, Baud, and Heap (2017). Although care was taken when performing manual measurements of sample dimensions (required in order to assess the sample porosity) both before and after the acid treatment, it is possible that experimental artifacts contribute to the scatter in our porosity data. We highlight that the error associated with any given porosity measurement (accounting for both the variability in sample dimensions and the variability of repeat pycnometry measurements) is $< \pm 0.0036$. However, propagation of potential error when dividing preimmersion and postimmersion measurements amplifies the overall error margin, as evident in Figure 4b. Nevertheless, porosity tends in general to increase over time, supporting the inference that acid immersion resulted in dissolution and removal (or remobilization) of mineral constituents of these andesites and in agreement with our SEM observations and solution analysis.

Indeed, microstructural evidence suggests not only that progressive dissolution of plagioclase phenocrysts took place (solubilizing elements such as Na, Ca, and Al and leaving behind the silica-rich phase: see Figures 5, 6, and 8) but also that interstitial glass of the groundmass was similarly dissolved in places (Figure 7). We suggest that the observed diktytaxitic microtextures—the porous frameworks of microlitic crystals—are evidence of acid-induced dissolution of the andesitic glass, whereby acid—in this case H_2SO_4—actively dissolves the glassy component of the pore walls, in turn creating more porosity and exposing new glass to the reactive fluid. We note that similar mechanisms have been invoked to account for diktytaxitic textures observed in natural samples: Horwell et al. (2013) and Schipper et al. (2015), for example, attribute such textures in rhyolite (from the 2011 Cordón Caulle eruption, Chile) to the scavenging of alkalis from the glass by magmagenic acids. In the case of neighboring pores (as in Figure 7b), development of the microporous network between them may greatly enhance pore connectivity (and hence permeability), without appreciably changing the overall void fraction of the rock (e.g., Kushnir et al., 2016). Notably, andesites from Volcán de Colima, Mexico—exhibiting similar textures—were observed to have specific surface areas of over 500 m^2/kg (determined using BET krypton adsorption): more than 10 times the value for other Volcán de Colima andesites with comparable total porosities (Farquharson et al., 2015). Similarly, andesites from Gunung Merapi, Indonesia were shown to have specific surface areas of up to almost 2,000 m^2/kg when the samples were diktytaxitic, compared to ~67 m^2/kg in juvenile material (Kushnir et al., 2016). However, we highlight that we did not here attempt a quantitative analysis of the spatial

evolution of diktytaxitic groundmass, nor can we confirm that the textures we observe in the postimmersion samples were not preexisting (indeed, we suggest that the differing apparent behavior of large plagioclase phenocrysts and microlites in response to acid exposure warrants future investigation). Previous studies have also highlighted the development of interfacial fracture planes along the encroaching silification front, recognized both in experiments (King et al., 2011) and in natural volcanic samples (Lowenstern et al., 2018). Such cracks are posited to serve as conduits for acid migration. Moreover, it has been demonstrated that such interfacial features—the development of ASSL in particular—can exert a first-order control on fluid–mineral interactions including the dissolution rate of silicate minerals, depending on the reactive conditions (e.g., Daval et al., 2013; Wild et al., 2016).

4.3. Dissolution and Permeability Change

Permeability is seen to increase markedly with progressive dissolution of the andesites examined in this study. As shown in Table 2 and Figure 4c, permeability of a sample immersed for 2,880 hr was measured to be over an order of magnitude greater than its initial value. Notably, the relatively large changes in permeability we measure are associated with only very slight porosity changes (Table 2). We have already suggested that acid-induced dissolution of the groundmass around pores may contribute to the large increase in permeability we observe. In particular, if the mean pore throat radius is influenced by prolonged exposure to acid, then this could greatly increase permeability directly, as well as the connectivity of porosity (indirectly associated with an increase in permeability).

As outlined in section 2, the measured permeability values were corrected for gas slippage after Klinkenberg (1941) and McPhee and Arthur (1991). The Klinkenberg, correction comprises a combination of Darcy's law (which describes fluid flow in porous media) and Poiseuille's law (which describes gas flow in capillaries). By unpacking the b term (equation (4)), we may estimate the mean radius $\bar{r}$ of flow pathways in our samples (the average pore radius of the flow path followed by the gas molecules; e.g., Heap et al., 2018). Klinkenberg (1941) shows that

$$\left(\frac{b}{\bar{p}}\right) = \left(\frac{4c\Lambda}{\bar{r}}\right) \tag{5}$$

where Λ is the mean-free path of gas molecules and c is a proportionality factor that can be assumed to equal 1. Moreover, after Loeb (1934), we can state that

$$\Lambda = \left[\frac{\mu}{\bar{p}}\right]\left[\left(\frac{\pi}{2}\right)\left(\frac{RT}{M}\right)\right]^{\frac{1}{2}}\left[\frac{2-f}{f}\right] \tag{6}$$

where μ is the gas viscosity, R is the ideal gas constant, T is temperature, and M is the molecular mass of the permeant gas. The parameter f corresponds to Maxwell's assumption that a fraction f of gas molecules are "absorbed" at the surface of a tubular capillary on collision; conversely, the proportion $1 - f$ molecules are assumed to be specularly reflected from the capillary wall (Loeb, 1934). For the purposes of our analysis, it can be assumed that $f = 1$; thus, the final segment of equation (6) is eliminated. All other parameters are as previously defined. By combining equations (5) and (6), we obtain

$$\bar{r} = \left[\frac{4\mu}{b}\right]\left[\left(\frac{\pi}{2}\right)\left(\frac{RT}{M}\right)\right]^{\frac{1}{2}} \tag{7}$$

which we can use to assess the relative aperture of flow pathways in our samples before and after acid immersion. Although equations (5)–(7) assume that flow occurs through a system of cylindrical capillaries—clearly an oversimplification of the complex microstructures exhibited by the andesites studied herein—this analysis can nonetheless tells us something about the evolution of the mean width of flow pathways as a function of acid immersion. Preimmersion and postimmersion values of the mean flow path radius, $\bar{r}$ and $\bar{r}^*$, respectively, are given in Table 3.

Clearly, the calculated mean pore radius increases with continued acid immersion time (Figure 9). Indeed, over the maximum duration of our experiments, $\bar{r}$ increases by a factor of 5 (Figure 9 and Table 3).

Understanding and modeling eruptive behavior in active volcanic systems rests on a knowledge of the physical and mechanical properties of the materials that form the edifice (e.g., Heap, Kennedy, et al., 2017). Given that acid-induced dissolution in the andesites of our study resulted in—among other changes—up to an order of magnitude increase in permeability, the capacity for physical property evolution in acidic volcanic

Table 3
Calculated Mean Pore Throat Radius Before $\bar{r}$ and After $\bar{r}^*$ Acid Immersion, From Equation (7)

Sample	$\bar{r}$ (μm)	$\bar{r}^*$ (μm)
MW-2	0.068	0.052
MW-4	0.064	0.070
MW-5	0.040	0.072
MW-6	0.110	0.146
MW-8	0.053	0.074
MW-11	0.094	0.132
MW-14	0.054	0.118
MW-17	0.025	0.074
MW-18	0.042	0.136
MW-19	0.041	0.201

environments may comprise an important consideration for such models. Indeed, while recent models of gas evolution in volcanic systems have tended to include the potential for spatially variable permeability (e.g., Collinson & Neuberg, 2012), temporal evolution of fluid flow capacity is often not parameterized.

Moreover, in a natural environment, it is reasonable to expect residence times of rocks in acid over far greater timescales. If magmatic volatiles are regularly replenished, permeability of volcanic media exposed to reactive fluid environments may continue to increase over time, provided dissolution continues to dominate over precipitation mechanisms, as was the case in our experiments. Conceptually, this may result in an overall reduction in short-term pressure development and to some extent promote quiescent behavior at active volcanoes. Nevertheless, we highlight that hydrothermal processes in volcanic settings may often result in the precipitation of mineral phases, not solely their dissolution (e.g., Heap, Kennedy, et al., 2017; Taran et al., 2000). Although this was not observed in our experiments, we note that hydrothermal mineral precipitation is expected to decrease permeability in general (e.g., Edmonds et al., 2003; Heap, Kennedy,

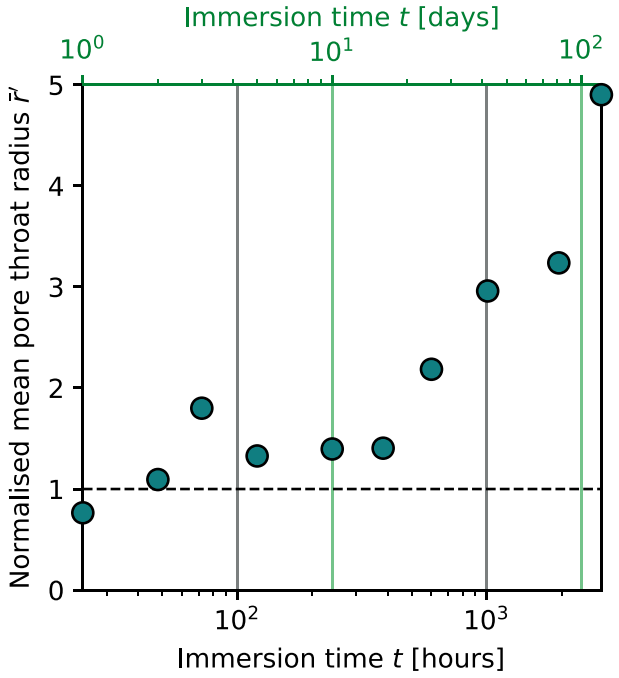

Figure 9. Calculated mean pore throat radii after acid immersion $\bar{r}^*$, normalized to their respective preimmersion values $\bar{r}$ after equation (7) to give $\bar{r}'$ against immersion time. As in Figure 4, values greater than 1 represent a relative increase of calculated mean pore radius, and values less than 1 indicate a relative decrease.

et al., 2017). Indeed, cyclic pressurization of volcanic conduits as a direct consequence of secondary mineral precipitation was speculated upon and modeled by Christenson et al. (2010).

Despite clear evidence of plagioclase dissolution, we do not see any compelling evidence for pyroxene dissolution based on our EDX data and SEM observations (e.g., Figure 6). In broad terms, the relative reactivity plagioclase > pyroxene is in agreement with previous research into element reactivity and acid-induced dissolution of volcanic material (e.g., Africano & Bernard, 2000; Delmelle & Bernard, 1994; Fang et al., 2003; Nogami & Yoshida, 1995; Rowe & Brantley, 1993; Sak et al., 2004, 2010). This is a promising outcome and suggests that a targeted quantitative analysis—using, for example, focused ion beam transmission electron microscopy, electron microprobe analysis, or time-resolved analysis of elemental release into solution by inductively coupled plasma atomic emission spectroscopy—would prove valuable for bridging the gap between microscale and macroscale processes in acidic volcanic environments. We acknowledge and emphasize that our experiments were not conducted at a scale appropriate for unraveling mineral-scale dissolution mechanisms; nevertheless, these observations highlight an interesting avenue for future research relating mineral-scale processes to the evolution of macroscopic physical and mechanical properties.

4.4. Strength Evolution and Volcanic Hazard

The weakening of volcanic rock through acid dissolution may comprise a significant hazard in many volcanic regions. Dissolution-induced weakening of edifice material has been posited to decrease edifice strength (e.g., Varekamp et al., 2001): assertions, which are borne out by our experimental data. Although the UCS data of samples that underwent acid immersion do not deviate significantly from the trend of unaltered samples (Figure 4d), their porosities are—in general—higher than prior to immersion. As such, sample strength decreases in line with the inverse relation illustrated in the figure. While the absolute porosity changes $\Delta\varphi$ observed during our experiment were modest (Table 2), dissolution in natural systems may of course occur over considerably longer timescales, hence increasing the potential for porosity creation and attendant weakening of volcanic rock. The fact that the compressive strength of samples that underwent acid treatment remains in the general trend is not unexpected: it has been shown by previous studies that the UCS of porous rocks is controlled not only by the overall sample porosity, but more specifically by the size of the largest pores (Baud et al., 2017; Zhu et al., 2016). Our microstructural analysis did not reveal significant changes in the macropore size, from which we infer that variations in strength are likely to be due to the overall change in porosity due to the exposure to acid. While our experiments were performed under atmospheric pressure conditions, it is worth noting that at depth (hence, under increased effective pressures), the concomitant increase of porosity and micropore size due to acid exposure is expected to have a relatively larger effect on the mechanical strength. Mechanical rock failure resulting from cataclastic pore collapse (a process expected to be common at depth in a volcanic edifice; Heap et al., 2015), is a function of effective pressure—which is to say, the in situ stress conditions within the edifice—and mean pore radius of the rock. After the model of Zhu et al. (2010), the effective pressure required for failure should decrease by a factor of $\sqrt{3}$ for an increase in mean pore radius by a factor of 3. As shown in Figure 9, this could be brought about after 1,000 hr of acid immersion. Essentially, this indicates that exposure of volcanic rock to acid may result in mechanical failure occurring under lower stress conditions than would be the case in the absence of acid-induced dissolution.

Varekamp et al. (2001) stress the hazard presented by alteration-induced flank collapse (and subsequent lahar generation) at Copahue volcano in Argentina, providing field evidence that such processes have occurred previously. Carrasco-Núñez et al. (1993) also determine a correlation between the degree of alteration of edifice rock and the incidence (or likelihood) of edifice collapse. Moreover, Carrasco-Núñez et al. (1993) emphasize that the existence of hydrothermally-altered rock greatly exacerbates the risk of cohesive lahar generation in active volcanic environments. The most destructive of lahars are often those that involve the sudden release of large volumes of water from crater lakes (Neall, 1976): a very real yet relatively underappreciated concern in many volcanic areas. Houghton et al. (1987) notes that one of the primary threats posed by Mount Ruapehu is the potential collapse of the southwestern rim of its apical crater (Figures 1a and 2a), a potential hazard that has prompted a number of recent investigative studies (e.g., Cook et al., 2017). The subsequent release of the lakewater is predicted to have a "catastrophic effect on the eastern and southeastern side of the mountain" (Houghton et al., 1987). In particular, permeability has been identified as a critical controlling parameter in stability models at Ruapehu (Schaefer et al., 2018): dissolution-driven increases in permeability coupled with a reduction in UCS could serve to lower the threshold for larger scale failure of the volcanic edifice (Schaefer et al., 2018). Such a collapse-induced lahar would certainly damage

critical transport links and other nearby infrastructure. The hazard posed by potential crater or caldera rim collapse has since also been recognized at other volcanoes, such as Aniakchak volcano, USA (Waythomas et al., 1996) and Rincón de la Vieja, Costa Rica (Kempter & Rowe, 2000). Indeed, as discussed by Waythomas et al. (1996), many lake-filled craters and calderas are elevated relative to the surrounding terrain, greatly exacerbating any flood or lahar risk for proximal communities.

5. Conclusion

Samples of andesite were immersed in a 0.125 M solution of H_2SO_4, analogous to an acidic volcanic lake system, for up to 2,880 hr (120 days). A progressive loss of mass was observed over time (up to 3% of the sample mass over the maximum timescale of our experiments), while porosity generally increased accordingly. Permeability was measured to increase by over an order of magnitude. These physical property changes are attributed to continued dissolution of plagioclase by the acid solution, accompanied by the generation of microporous diktytaxitic groundmass textures due to glass dissolution. Plagioclase phenocrysts are replaced by a pseudomorphic Si-rich phase as cations are solubilized. At first (t = 24–240 hr), this process appears to be confined primarily to preexisting fractures within the crystals. However, ultimately these phenocrysts are almost entirely replaced by amorphous silica while retaining their initial shapes. Residual plagioclase appears as isolated islands within the pseudomorphic phase. We do not observe evidence of induced dissolution or alteration in the other mineral constituents of the material: pyroxene, cristobalite, and titanomagnetite, specifically. Based on our observations, we calculate an increase in the mean pore radius of up to a factor of 5, which corresponds well with acid immersion time. From this we infer that acid-induced dissolution serves to widen the narrowest pore throat apertures over time. UCS of these andesites is also affected, insofar as porosity evolves as a function of acid-induced dissolution and porosity and strength are inversely correlated. Ultimately, we assess that the samples immersed in a H_2SO_4 acid solution were weaker than they otherwise would have been. The increase in permeability and reduction in strength have implications for outgassing capacity and stability of volcanic edifices.

Acknowledgments
Data are available in Tables 1 –3. The authors of this study acknowledge a Dumont d'Urville Hubert Curien Partnership (PHC) grant (31950RK), implemented in France by the Ministry of Europe and Foreign Affairs (MEAE) and the Ministry of Higher Education, Research and Innovation (MESRI), and in New Zealand by the Ministry of Business, Innovation and Employment (MBIE) and the Royal Society of New Zealand. This project was funded in part by the framework of the LABEX ANR-11-LABX-0050_G-EAU-THERMIE-PROFONDE and therefore benefits from a funding from the state managed by the French National Research Agency as part of the Programme d'Investissements d'Avenir ("Investments for the future" program). B. W. was supported by Princeton University's Andlinger Center for Energy and Environment through its Distinguished Postdoctoral Fellows program. H. A. Gilg is acknowledged for performing the XRPD measurements. Bertrand Renaudié is thanked for sample preparation, Thierry Reuschlé is thanked for technical assistance, and Damien Daval is acknowledged for insightful discussions. B. K. acknowledges the funds supplied by natural hazards research platform "Quantifying exposure to specific and multiple volcanic hazards" for his part in the research. We are grateful to Maarten de Moor and Anthony Lamur for their constructive feedback on the manuscript. Finally, we would like to acknowledge Department of Conservation New Zealand for their assistance with permitting and access, and we would like to acknowledge the people of Ngāti Tūwharetoa and Ngāti Rangi for their support of our work on Mount Ruapehu, which has great cultural significance.

References

Africano, F., & Bernard, A. (2000). Acid alteration in the fumarolic environment of Usu volcano, Hokkaido, Japan. *Journal of Volcanology and Geothermal Research*, *97*(1-4), 475–495.

Armienta, M., De la Cruz-Reyna, S., & Macıas, J. (2000). Chemical characteristics of the crater lakes of Popocatetetl, El Chichon, and Nevado de Toluca volcanoes, Mexico. *Journal of Volcanology and Geothermal Research*, *97*(1-4), 105–125.

Ashwell, P., Kendrick, J., Lavallée, Y., Kennedy, B., Hess, K.-U., Aulock, F., et al. (2015). Permeability of compacting porous lavas. *Journal of Geophysical Research: Solid Earth*, *120*, 1605–1622. https://doi.org/10.1002/2014JB011519

Ball, J. L., Calder, E. S., Hubbard, B. E., & Bernstein, M. L. (2013). An assessment of hydrothermal alteration in the Santiaguito lava dome complex, Guatemala: Implications for dome collapse hazards. *Bulletin of Volcanology*, *75*(1), 676.

Ball, J. L., Stauffer, P. H., Calder, E. S., & Valentine, G. A. (2015). The hydrothermal alteration of cooling lava domes. *Bulletin of Volcanology*, *77*(12), 102.

Baud, P., Exner, U., Lommatzsch, M., Reuschlé, T., & Wong, T.-f. (2017). Mechanical behavior, failure mode, and transport properties in a porous carbonate. *Journal of Geophysical Research: Solid Earth*, *122*, 7363–7387. https://doi.org/10.1002/2017JB014060

Bernard, A., Escobar, C. D., Mazot, A., & Gutiérrez, R. E. (2004). The acid volcanic lake of Santa Ana volcano, El Salvador. *Geological Society of America, Special Paper*, *375*, 121–134.

Carrasco-Núñez, G., Vallance, J. W., & Rose, W. I. (1993). A voluminous avalanche-induced lahar from Citlaltépetl volcano, Mexico: Implications for hazard assessment. *Journal of Volcanology and Geothermal Research*, *59*(1-2), 35–46.

Casadevall, T. J., De la Cruz-Reyna, S., W. I. Rose Jr, Bagley, S., Finnegan, D. L., & Zoller, W. H. (1984). Crater lake and post-eruption hydrothermal activity, El Chichón volcano, Mexico. *Journal of Volcanology and Geothermal Research*, *23*(1-2), 169–191.

Christenson, B., Reyes, A., Young, R., Moebis, A., Sherburn, S., Cole-Baker, J., & Britten, K. (2010). Cyclic processes and factors leading to phreatic eruption events: Insights from the 25 September 2007 eruption through Ruapehu crater lake, New Zealand. *Journal of Volcanology and Geothermal Research*, *191*(1-2), 15–32.

Christenson, B. W., White, S., Britten, K., & Scott, B. J. (2017). Hydrological evolution and chemical structure of a hyper-acidic spring-lake system on Whakaari/White Island, NZ. *Journal of Volcanology and Geothermal Research*, *346*, 180–211.

Christenson, B., & Wood, C. (1993). Evolution of a vent-hosted hydrothermal system beneath Ruapehu crater lake, New Zealand. *Bulletin of volcanology*, *55*(8), 547–565.

Collinson, A., & Neuberg, J. (2012). Gas storage, transport and pressure changes in an evolving permeable volcanic edifice. *Journal of Volcanology and Geothermal Research*, *243*, 1–13.

Colombier, M., Wadsworth, F. B., Gurioli, L., Scheu, B., Kueppers, U., Di Muro, A., & Dingwell, D. B. (2017). The evolution of pore connectivity in volcanic rocks. *Earth and Planetary Science Letters*, *462*, 99–109.

Cook, S. C., Kennedy, B. M., & Villeneuve, M. C. (2017). Engineering geology model of the crater lake outlet, Mt. Ruapehu, New Zealand, to inform rim breakout hazard. *Journal of Volcanology and Geothermal Research*, *350*, 69–83.

Damby, D. E., Llewellin, E. W., Horwell, C. J., Williamson, B. J., Najorka, J., Cressey, G., & Carpenter, M. (2014). The α–β phase transition in volcanic cristobalite. *Journal of applied crystallography*, *47*(4), 1205–1215.

Daval, D., Hellmann, R., Saldi, G. D., Wirth, R., & Knauss, K. G. (2013). Linking nm-scale measurements of the anisotropy of silicate surface reactivity to macroscopic dissolution rate laws: New insights based on diopside. *Geochimica et Cosmochimica Acta*, *107*, 121–134.

de Moor, J., Aiuppa, A., Pacheco, J., Avard, G., Kern, C., Liuzzo, M., et al. (2016). Short-period volcanic gas precursors to phreatic eruptions: Insights from Poás volcano, Costa Rica. *Earth and Planetary Science Letters*, *442*, 218–227. https://doi.org/10.1016/j.epsl.2016.02.056

Delmelle, P., & Bernard, A. (1994). Geochemistry, mineralogy, and chemical modeling of the acid crater lake of Kawah Ijen volcano, Indonesia. *Geochimica et cosmochimica acta*, *58*(11), 2445–2460.

Delmelle, P., & Bernard, A. (2000). Volcanic lakes. In *Encyclopedia of volcanoes* (pp. 877–896). San Diego: Academic Press.

Edmonds, M., & Herd, R. A. (2007). A volcanic degassing event at the explosive-effusive transition. *Geophysical Research Letters*, *34*, L21310. https://doi.org/10.1029/2007GL031379

Edmonds, M., Oppenheimer, C., Pyle, D., Herd, R., & Thompson, G. (2003). So_2 emissions from Soufrière Hills volcano and their relationship to conduit permeability, hydrothermal interaction and degassing regime. *Journal of Volcanology and Geothermal Research*, *124*(1), 23–43.

Eichelberger, J., Carrigan, C., Westrich, H., & Price, R. (1986). Non-explosive silicic volcanism. *Nature*, *323*(6089), 598–602.

Fang, J.-N., Lo, H.-J., Song, S.-R., Chung, S.-H., Chen, Y.-L., Lin, I., et al. (2003). Hydrothermal alteration of andesite in acid solutions: Experimental study in 0.05 m H_2SO_4 solution at 110°C. *Journal of the Chinese Chemical Society*, *50*(2), 239–244.

Farquharson, J. I., Baud, P., & Heap, M. J. (2017). Inelastic compaction and permeability evolution in volcanic rock. *Solid Earth*, *8*(2), 561–581.

Farquharson, J. I., Heap, M. J., Varley, N. R., Baud, P., & Reuschlé, T. (2015). Permeability and porosity relationships of edifice-forming andesites: A combined field and laboratory study. *Journal of Volcanology and Geothermal Research*, *297*, 52–68.

Farquharson, J. I., Wadsworth, F. B., Heap, M. J., & Baud, P. (2017). Time-dependent permeability evolution in compacting volcanic fracture systems and implications for gas overpressure. *Journal of Volcanology and Geothermal Research*, *339*, 81–97.

Gaunt, H. E., Bernard, B., Hidalgo, S., Proaño, A., Wright, H., Mothes, P., et al. (2016). Juvenile magma recognition and eruptive dynamics inferred from the analysis of ash time series: The 2015 reawakening of Cotopaxi volcano. *Journal of Volcanology and Geothermal Research*, *328*, 134–146.

Heap, M. J., Farquharson, J. I., Baud, P., Lavallée, Y., & Reuschlé, T. (2015). Fracture and compaction of andesite in a volcanic edifice. *Bulletin of volcanology*, *77*(6), 55.

Heap, M. J., Kennedy, B. M., Farquharson, J. I., Ashworth, J., Mayer, K., Letham-Brake, M., et al. (2017). A multidisciplinary approach to quantify the permeability of the Whakaari/White Island volcanic hydrothermal system (Taupo volcanic zone, New Zealand). *Journal of Volcanology and Geothermal Research*, *332*, 88–108.

Heap, M. J., Kushnir, A. R., Gilg, H. A., Wadsworth, F. B., Reuschlé, T., & Baud, P. (2017). Microstructural and petrophysical properties of the Permo-Triassic sandstones (Buntsandstein) from the Soultz-sous-Forêts geothermal site (France). *Geothermal Energy*, *5*(1), 26.

Heap, M., Lavallée, Y., Petrakova, L., Baud, P., Reuschle, T., Varley, N., & Dingwell, D. B. (2014). Microstructural controls on the physical and mechanical properties of edifice-forming andesites at Volcán de Colima, Mexico. *Journal of Geophysical Research: Solid Earth*, *119*, 2925–2963. https://doi.org/10.1002/2013JB010521

Heap, M., Reuschlé, T., Farquharson, J., & Baud, P. (2018). Permeability of volcanic rocks to gas and water. *Journal of Volcanology and Geothermal Research*, *354*, 29–38.

Hemley, J. J., & Jones, W. (1964). Chemical aspects of hydrothermal alteration with emphasis on hydrogen metasomatism. *Economic Geology*, *59*(4), 538–569.

Horwell, C. J., Williamson, B. J., Llewellin, E. W., Damby, D. E., & Le Blond, J. S. (2013). The nature and formation of cristobalite at the Soufrière Hills volcano, Montserrat: Implications for the petrology and stability of silicic lava domes. *Bulletin of Volcanology*, *75*(3), 696.

Houghton, B., Latter, J., & Hackett, W. (1987). Volcanic hazard assessment for Ruapehu composite volcano, Taupo volcanic zone, New Zealand. *Bulletin of volcanology*, *49*(6), 737–751.

Kawano, M., & Tomita, K. (2001). TEM-EDX study of weathered layers on the surface of volcanic glass, bytownite, and hypersthene in volcanic ash from Sakurajima volcano, Japan. *American Mineralogist*, *86*(3), 284–292.

Kempter, K., & Rowe, G. (2000). Leakage of active crater lake brine through the north flank at Rincón de la Vieja volcano, northwest Costa Rica, and implications for crater collapse. *Journal of Volcanology and Geothermal Research*, *97*(1-4), 143–159.

King, H. E., Plümper, O., Geisler, T., & Putnis, A. (2011). Experimental investigations into the silicification of olivine: Implications for the reaction mechanism and acid neutralization. *American Mineralogist*, *96*(10), 1503–1511.

Klinkenberg, L. (1941). The permeability of porous media to liquids and gases, *Drilling and production practice*. New York: American Petroleum Institute.

Kusakabe, M., Komoda, Y., Takano, B., & Abiko, T. (2000). Sulfur isotopic effects in the disproportionation reaction of sulfur dioxide in hydrothermal fluids: Implications for the δ^{34} S variations of dissolved bisulfate and elemental sulfur from active crater lakes. *Journal of Volcanology and Geothermal Research*, *97*(1-4), 287–307. https://doi.org/10.1016/s0377-0273(99)00161-4

Kushnir, A. R., Martel, C., Bourdier, J.-L., Heap, M. J., Reuschlé, T., Erdmann, S., et al. (2016). Probing permeability and microstructure: Unravelling the role of a low-permeability dome on the explosivity of Merapi (Indonesia). *Journal of Volcanology and Geothermal Research*, *316*, 56–71.

Loeb, L. B. (1934). *The kinetic theory of gases Ed. 2*. New York: Mcgrew-hill Book Co.

Lowenstern, J. B., van Hinsberg, V., Berlo, K., Liesegang, M., Iacovino, K., Bindeman, I., & Wright, H. M. (2018). Opal-a in glassy pumice, acid alteration, and the 1817 phreatomagmatic eruption at Kawah Ijen (Java), Indonesia. *Frontiers in Earth Science*, *6*, 11.

Manville, V., Hodgson, K., & Nairn, I. (2007). A review of break-out floods from volcanogenic lakes in New Zealand. *New Zealand Journal of Geology and Geophysics*, *50*(2), 131–150.

Massiot, C. (2017). Fracture system characterisation and implications for fluid flow in volcanic and metamorphic rocks (Ph.D. thesis), Victoria University of Wellington.

McPhee, C. A., & Arthur, K. G. (1991). Klinkenberg permeability measurements: Problems and practical solutions. In *Advances in Core Evaluation IL Reservoir Appraisal, Proceedings of the 2nd Society of Core Analysts European Core Analysis Symposium, Gordon & Breach Science Publishers, Philadelphia*, pp. 371–391.

Michaelis, F. B. (1982). The lake of Tongariro National Park. *Mauri Ora*, *10*, 49–65.

Minami, Y., Imura, T., Hayashi, S., & Ohba, T. (2016). Mineralogical study on volcanic ash of the eruption on September 27, 2014 at Ontake volcano, central Japan: Correlation with porphyry copper systems. *Earth, Planets and Space*, *68*(1), 67.

Nakamura, K. (1977). Volcanoes as possible indicators of tectonic stress orientation—Principle and proposal. *Journal of Volcanology and Geothermal Research*, *2*(1), 1–16.

Neall, V. (1976). Lahars as major geological hazards. *Bulletin of the International Association of Engineering Geology-Bulletin de l'Association Internationale de Géologie de l'Ingénieur*, *13*(1), 233–240.

Nguyen, C. T., Gonnermann, H. M., & Houghton, B. F. (2014). Explosive to effusive transition during the largest volcanic eruption of the 20th century (Novarupta 1912, alaska). *Geology*, *42*(8), 703–706.

Nogami, K., & Yoshida, M. (1995). Leaching rates of rock-forming components through acidic alteration. *Journal of Volcanology and Geothermal Research*, *65*(1-2), 41–49.
O'Shea, B. E. (1957). Contributions to the geology of Mt. Ruapehu, New Zealand.
Okumura, S., & Sasaki, O. (2014). Permeability reduction of fractured rhyolite in volcanic conduits and its control on eruption cyclicity. *Geology*, *42*(10), 843–846.
Perez, N. M., Hernandez, P. A., Padilla, G., Nolasco, D., Barrancos, J., Melian, G., et al. (2011). Global CO_2 emission from volcanic lakes. *Geology*, *39*(3), 235–238. https://doi.org/10.1130/g31586.1
Putnis, A. (2009). Mineral replacement reactions. *Reviews in Mineralogy and Geochemistry*, *70*(1), 87–124.
Reid, M. E., Keith, T. E., Kayen, R. E., Iverson, N. R., Iverson, R. M., & Brien, D. L. (2010). Volcano collapse promoted by progressive strength reduction: New data from Mount St. Helens. *Bulletin of Volcanology*, *72*(6), 761–766.
Reid, M. E., Sisson, T. W., & Brien, D. L. (2001). Volcano collapse promoted by hydrothermal alteration and edifice shape, Mount Rainier, Washington. *Geology*, *29*(9), 779–782.
Rodríguez, A., & van Bergen, M. J. (2017). Superficial alteration mineralogy in active volcanic systems: An example of Poás volcano, Costa Rica. *Journal of Volcanology and Geothermal Research*, *346*, 54–80.
Rouwet, D., Taran, Y., Inguaggiato, S., Varley, N., & Santiago, J. S. (2008). Hydrochemical dynamics of the "lake–spring" system in the crater of El Chichón volcano (Chiapas, Mexico). *Journal of Volcanology and Geothermal Research*, *178*(2), 237–248.
Rowe, G. L., & Brantley, S. L. (1993). Estimation of the dissolution rates of andesitic glass, plagioclase and pyroxene in a flank aquifer of Poas volcano, Costa Rica. *Chemical Geology*, *105*(1-3), 71–87.
Rust, A., Cashman, K., & Wallace, P. (2004). Magma degassing buffered by vapor flow through brecciated conduit margins. *Geology*, *32*(4), 349–352.
Sak, P. B., Fisher, D. M., Gardner, T. W., Murphy, K., & Brantley, S. L. (2004). Rates of weathering rind formation on Costa Rican basalt. *Geochimica et Cosmochimica Acta*, *68*(7), 1453–1472.
Sak, P. B., Navarre-Sitchler, A. K., Miller, C. E., Daniel, C. C., Gaillardet, J., Buss, H. L., et al. (2010). Controls on rind thickness on basaltic andesite clasts weathering in Guadeloupe. *Chemical Geology*, *276*(3-4), 129–143.
Schaefer, LN., Kennedy, B. N., Villeneuve, M. C., Cook, S. C. W., Jolly, A., Keys, H., & Leonard, G. (2018). Stability assessment of the Crater Lake/Te Wai-ā-moe overflow channel at Mt. Ruapehu (New Zealand), and implications for volcanic lake break-out triggers. *Journal of Volcanology and Geothermal Research*, *358*, 31–44.
Schipper, C. I., Castro, J. M., Tuffen, H., Wadsworth, F. B., Chappell, D., Pantoja, A. E., et al. (2015). Cristobalite in the 2011-2012 Cordón Caulle eruption (Chile). *Bulletin of Volcanology*, *77*(5), 19.
Sparks, R. S. J. (1978). The dynamics of bubble formation and growth in magmas: A review and analysis. *Journal of Volcanology and Geothermal Research*, *3*(1-2), 1–37.
Taran, Y. A., Bernard, A., Gavilanes, J.-C., & Africano, F. (2000). Native gold in mineral precipitates from high-temperature volcanic gases of Colima volcano, Mexico. *Applied Geochemistry*, *15*(3), 337–346.
Timperley, M., & Vigor-Brown, R. (1986). Water chemistry of lakes in the Taupo volcanic zone, New Zealand. *New Zealand Journal of Marine and Freshwater Research*, *20*(2), 173–183.
Varekamp, J. C., Ouimette, A. P., Herman, S. W., Bermúdez, A., & Delpino, D. (2001). Hydrothermal element fluxes from Copahue, Argentina: A "beehive" volcano in turmoil. *Geology*, *29*(11), 1059–1062.
Varekamp, J., Pasternack, G., & Rowe, G. Jr. (2000). Volcanic lake systematics: II. Chemical constraints. *Journal of Volcanology and Geothermal Research*, *97*(1-4), 161–179.
Waythomas, C. F., Walder, J. S., McGimsey, R. G., & Neal, C. A. (1996). A catastrophic flood caused by drainage of a caldera lake at Aniakchak volcano, Alaska, and implications for volcanic hazards assessment. *Geological Society of America Bulletin*, *108*(7), 861–871.
Wild, B., Daval, D., Guyot, F., Knauss, K. G., Pollet-Villard, M., & Imfeld, G. (2016). pH-dependent control of feldspar dissolution rate by altered surface layers. *Chemical Geology*, *442*, 148–159.
Woods, A. W., & Koyaguchi, T. (1994). Transitions between explosive and effusive eruptions of silicic magmas. *Nature*, *370*, 641–644.
Zhu, W., Baud, P., Vinciguerra, S., & Wong, T.-f. (2016). Micromechanics of brittle faulting and cataclastic flow in Mount Etna basalt. *Journal of Geophysical Research: Solid Earth*, *121*, 4268–4289. https://doi.org/10.1002/2016JB012826
Zhu, W., Baud, P., & Wong, T.-f. (2010). Micromechanics of cataclastic pore collapse in limestone. *Journal of Geophysical Research*, *115*, B04405. https://doi.org/10.1029/2009JB006610